Data report: tectonic and induced structures in the JFAST core[1]

Tucker T. Keren[2] and James D. Kirkpatrick[2, 3]

Chapter contents

[1]Keren, T.T., and Kirkpatrick, J.D., 2016. Data report: tectonic and induced structures in the JFAST core. *In* Chester, F.M., Mori, J., Eguchi, N., Toczko, S., and the Expedition 343/343T Scientists, *Proceedings of the Integrated Ocean Drilling Program,* 343/343T: Tokyo (Integrated Ocean Drilling Program Management International, Inc.). doi:10.2204/iodp.proc.343343T.204.2016
[2]Department of Geosciences, Colorado State University, 1482 Campus Delivery, Fort Collins CO 80523, USA. Correspondence author: tuckerkeren@gmail.com
[3]Presently at: Department of Earth and Planetary Sciences, McGill University, 3450 University Street, Montreal QC H3A0E8, Canada.

Abstract

Structures surrounding the inferred location of the Japan Trench plate boundary décollement define the fault damage zone. We quantify the density of tectonic and induced structures in the damage zone from drill cores collected between 770 and 835 meters below seafloor from Hole C0019E during Integrated Ocean Drilling Program Expedition 343/343T, the Japan Trench Fast Drilling Project (JFAST). Cores contain structures formed by tectonic deformation and structures resulting from drill core recovery and handling. Differentiating between these two origins is essential for structural analyses and interpretation. We defined 10 styles of induced structures that we used to develop a new set of criteria for identifying induced structures in drill cores containing fine-grained sedimentary rocks. These criteria were used to categorize structures according to confidence in a tectonic origin. Our results show structure density (including all fractures, faults, breccias, and phyllosilicate bands) has a maximum adjacent to the décollement. This pattern in structure density is apparent for both exclusively tectonic structures and tectonic and induced structures combined. Local increases in induced structure density mask trends in tectonic structures, demonstrating that detecting trends in spatial variability in structure density is dependent on the recognition of induced structures. Additionally, the tectonic structure density increases where cores contain faults with significant displacements inferred from stratigraphic information, indicating that tectonic structure density can be used to identify secondary faults. We suggest that the criteria for identifying induced structures used in this study could be applied during visual core description in a variety of tectonic settings as a method to collect and assess reliable structural data.

Introduction

Coseismic thrust displacement during the 2011 Tohoku-Oki Mw 9.0 earthquake reached ~40–80 m near the trench, the largest slip ever recorded for an earthquake (Fujiwara et al., 2011; Fujii et al., 2011; Ide et al., 2011; Lay et al., 2011; Pollitz et al., 2011; Yue and Lay, 2011). Integrated Ocean Drilling Program (IODP) Expedition 343/343T (the Japan Trench Fast Drilling Project [JFAST] project) sailed 1 y after the earthquake to investigate the conditions and mechanisms that facilitated large, shallow slip. The primary goals

doi:10.2204/iodp.proc.343343T.204.2016

of the JFAST project included identifying and sampling the rocks that were deformed during the earthquake to establish the processes active on the fault during slip and to establish the stress state on the fault before, during, and after the earthquake (Mori et al., 2012). Structural data are critical for locating the plate boundary décollement, where both long-term and coseismic displacements are typically localized. The attitudes of fractures and faults around the fault also provide information about the stress field when they formed (see the **"Expedition 343/343T summary"** chapter [Expedition 343/343T Scientists, 2013a]).

Drilling was undertaken at Site C0019, ~7 km landward of the trench in the region of maximum slip during the earthquake (Fig. **F1**) (see the **"Expedition 343/343T summary"** chapter [Expedition 343/343T Scientists, 2013a]). Cores were recovered at targeted intervals from Hole C0019E, and onboard visual core description followed standard IODP procedures (see the **"Methods"** chapter [Expedition 343/343T Scientists, 2013b]). Tectonic structures including Mode I fractures, phyllosilicate bands, shear fractures, secondary faults, and breccia zones were logged, and care was taken to differentiate drilling-induced deformation in the core from tectonic features.

Distinguishing tectonic structures from those induced by drilling and recovery processes is a key goal of visual core description but is difficult because tectonic and human-induced deformation may appear alike. Drilling mud may also resemble natural features and sediments. Moreover, structures in weak sedimentary rock, like those recovered during the JFAST expedition, can show very little mineralization, therefore increasing the difficulty of distinguishing natural from induced damage. Of the published guidelines for identifying induced damage in core (e.g., Pendexter and Rohn, 1954; Kidd, 1978; Kulander et al., 1979, 1990; Dengo, 1982; Leggett, 1982; Lundberg and Moore, 1986), few address induced damage in mudstones.

Results from Expedition 343/343T onboard visual core description provided insufficient data for robust estimates of the spatial distribution or orientation of structures throughout the frontal prism and in particular surrounding the plate boundary fault (see the **"Expedition 343/343T summary"** chapter [Expedition 343/343T Scientists, 2013a]; Kirkpatrick et al., 2015). Here, we reexamine the cores from Hole C0019E with the aims of (1) expanding on previous criteria for distinguishing induced and tectonic deformation to (2) evaluate the spatial variability of tectonic structure density and (3) establish whether structure density can be used to locate fault horizons as observed in IODP cores elsewhere (e.g., Brown and Behrmann, 1990; Maltman et al., 1993; Ujiie and Kimura, 2014).

Cores from Hole C0019E used for analysis

Twenty-one cores were recovered from Hole C0019E from the following depth intervals: 176.5–185.2, 648–660, ~690–725, and ~770–835 meters below seafloor (mbsf), with an overall recovery rate of 43%. The first 16 coring runs recovered rocks composed of Pliocene and Pleistocene siliceous mudstones of the hanging wall frontal prism (see the **"Expedition 343/343T summary"** chapter [Expedition 343/343T Scientists, 2013a]; Rabinowitz et al., 2015). Section 17R-1 is composed of highly sheared scaly clay interpreted to be the plate boundary décollement (821.5–822.5 mbsf) (see the **"Expedition 343/343T summary"** chapter [Expedition 343/343T Scientists, 2013a]; Rabinowitz et al., 2015). Below the décollement, rocks include middle to late Miocene brown siliceous mudstone, early Miocene stratified pelagic clay, and Late Cretaceous laminar chert at the total drilling depth (see the **"Expedition 343/343T summary"** chapter [Expedition 343/343T Scientists, 2013a]; Rabinowitz et al., 2015). Degree of lithification increases moderately with depth, indicated by increasing *P*-wave velocity (meters per second) and electrical resistivity (ohm-meters) (see the **"Expedition 343/343T summary"** chapter [Expedition 343/343T Scientists, 2013a]; Nakamura et al., 2014). Unconfined compressive strength of recovered rocks also increases with depth, ranging from 1 to 10 MPa (see the **"Expedition 343/343T summary"** chapter [Expedition 343/343T Scientists, 2013a]). All examined cores contained intact rock; the most poorly lithified units were pelagic clay, whereas the most well lithified units were chert.

The data reported here focus on deformation hypothesized to define the damage zone surrounding the plate boundary décollement, rather than all 21 cores collected from Hole C0019E. A damage zone is generally defined as the network of subsidiary structures—faults, fractures, and veins—that bound a fault core and are related to the development of the fault (e.g., Chester and Logan, 1986; Caine et al., 1996). Our study focuses on subsidiary structures in Cores 10R–20R, which surround the décollement and were recovered from 770 to 833.5 mbsf. We examined a total of 6.73 m of intact core below the décollement and a total of 9.38 m of intact core above the décollement. The total depth interval examined in this study is 63.5 m.

Methods

Distinguishing tectonic and induced deformation

Tectonic deformation in drill core includes the structures present in the volume of rock prior to drilling. Here, we use a set of criteria to identify tectonic deformation based on kinematic and geometric evidence following methods practiced on board during Expedition 343. Characteristics of tectonic structures in the split core face include the following:

- Shear displacement evidenced by measurable offset of piercing points such as marker beds or other predeformational structures, truncation of marker beds or other tectonic structures where displacement may exceed core width, development of slickenlines on fracture surface planes, or significant changes in bedding orientation across a structure, or juxtaposition of different rock types/chemistries/fossil assemblages.
- Development of fault rock formed by deformation within a brittle shear zone (e.g., scaly fabric defined by the surfaces of phacoid lenses that create an anastomosing network of curviplanar, striated shear surfaces) or as an alternative to scaly fabric, a nonfoliated fault gouge.
- Presence of tectonic breccia (which may occur without independent evidence for shear displacement) indicated by striated and/or polished surfaces on subangular to angular fragments or by gradational boundaries defined by less fractured rock.
- Formation of anastomosing or braided networks of structures dark gray to black in color, often with higher X-ray computed tomography (X-CT) numbers (indicating increase in density) than the surrounding rock, with orientations typically oblique to bedding (i.e., phyllosilicate bands [Fossen et al., 2007]).
- Fracture fill or mineralization evidenced by change in color or mineralogy within structure compared to surrounding rock.
- Consistent orientation(s) of adjacent structures that define structure sets likely forming under the same stress field.

Induced deformation in core includes structures that form as a result of drilling, coring, or handling operations. Kulander et al. (1990) provide a detailed description of common induced structures observed in drill core, which fall into three categories: drilling-induced structures that propagate in the rock ahead of the drill bit, coring-induced structures that develop anywhere within the core barrel, and handling-induced structures that form during or after removal of the core from the core barrel. Drilling- and coring-induced structures are initiated by stresses related to drilling operations and/or removal of overburden pressure. Handling-induced structures are initiated by stresses related to splitting, bending, and impact after cores are brought on board (Kulander et al., 1990).

Whereas the groupings defined by Kulander et al. (1990) provide a simple overview of induced structure types, complexity arises when core recovery results in open fractures forming along preexisting in situ tectonic structures or sedimentary layering. Therefore, an open fracture in recovered core may be a primary tectonic structure, an induced feature, or an induced fracture superimposed on a primary structure and/or preexisting mechanical anisotropy. Examples of preexisting mechanical anisotropies include natural fractures, faults, microfractures, bedding planes, residual stresses, and solution cleavage (Kulander et al., 1990).

We defined 10 styles of induced deformation from a combination of our observations of the split faces of Hole C0019E cores and previously published descriptions of induced deformation. The definitions of each and the criteria employed to identify them are described below.

Drilling biscuits/discs

Drilling biscuits or discs ("biscuits") are one of the most commonly recognized examples of induced damage in core. Following observations made by Pendexter and Rohn (1954), Kidd (1978) first cataloged induced damage observations with a focus on "core-discing" in the context of deep-sea drilling after encountering examples in Deep Sea Drilling Project (DSDP) Leg 42A Mediterranean sediment cores. Biscuits appear as separated blocks with convex tops and/or concave bottoms (Fig. **F2A**), typically separated by drilling mud or a collection of rock fragments in a matrix of drilling mud. Drilling mud can also smear along the side of the core and out from between biscuits, resulting in discrete, isolated biscuits of lithified material (Leggett, 1982). Inclinations of biscuit edges are typically horizontal to subhorizontal in vertical or subvertical cores; however, inclined bedding can influence the orientation (Kulander et al., 1990). Completely developed horizontal coring-induced biscuits cut entirely across the core or abut against earlier-formed natural or coring-induced structures (Kulander et al., 1979). Additionally, circular striations can sometimes be observed on the tops and/or bottoms of biscuits.

Biscuiting is the result of vertical tensile stress acting on the rock during progress of the drill bit followed by blocks spinning with respect to each other in the

core barrel (Kidd, 1978; Kulander et al., 1979). Rapid removal of overlying strata permits underlying rocks to expand, contributing to vertical tension and the formation of subhorizontal fractures due to unloading. It common for some biscuits to be held steady in the core barrel while other adjacent biscuits rotate with the drill. Curved edges form as the biscuits spin while staying in contact with each other (e.g., Kidd, 1978). The wear and abrasion results in erosion of biscuit edges and local formation of wear products that may resemble fault gouge or drilling mud.

Induced brecciation

The term "induced breccia" is commonly used in visual core description because of the tendency for drilling operations to recover cores that contain only fragmented angular clasts. For a clear example, see Cores 2R and 3R. Throughout the majority of cores from Hole C0019E, however, induced breccia clasts appear within a single biscuit, as if each fragment is a uniquely fitting piece of a puzzle, or in between biscuits in random orientations. More simply, others have described drilling breccias as angular chips of indurated mudstone in drilling mud (Leggett, 1982). One reliable way to differentiate between natural tectonic brecciation and drilling-induced brecciation is the presence of striations on individual clasts. Induced breccias will sometimes lack slickenlines or polished surfaces because of limited relative motion between clasts. An exception is spiral or helicoidal slickenlines resulting from the biscuiting process (see the **"Methods"** chapter [Expedition 343/343T Scientists, 2013b]). Most induced brecciation observed in Hole C0019E cores is not in a matrix of drilling mud, such as the induced breccia zone in Figure **F2B,** where none of the angular clasts exhibit slickenlines or polished surfaces between pieces.

Triangular fracture sets

Triangular fracture sets are common at the edge of the core barrel in the split face of the core. Triangular fracture sets are typically defined by subhorizontal fractures dipping in opposite directions that intersect at the apex of a triangle that points toward the center of the core (Fig. **F2C**). These structures are interpreted as induced because their orientations locally parallel biscuit edges and/or other induced structure orientations and the triangular geometry is consistent with localized failure during vertical flexing of the core (e.g., Hiraishi, 1984). The triangles can occur at nearly all scales visible within the core. The angle at the apex between the two fractures in a triangular geometry ranges from ~30° (Fig. **F2C**) to over 100° (Fig. **F2D**). A complicating factor in determining the origin of fractures that make triangles at the edge of the drill core is the case of reactivation of tectonic fractures. In some cases, fractures with triangular geometries trend directly into tectonic structures, most commonly phyllosilicate bands (Fig. **F2E**). Triangular fracture sets can sometimes form in between two biscuits and because flexure of the core in the vertical direction ultimately erode away (Fig. **F2C**).

(Near) right-angle fractures

Continuous, open fractures exhibiting nearly 90° bends are prevalent near the outer edge of Hole C0019E drill cores. The most common occurrence of such fractures is along biscuit corners. Right-angle fractures are observed both opening along preexisting tectonic structures and with no adjacent or parallel tectonic structures (Fig. **F2F**). In the absence of any evidence of shear or abutting relationships between the differently oriented segments of a right-angle fracture, we infer that they are the result of continued rotation and flexure of the core, resulting in removal of corners from biscuits. As described in Kulander et al. (1990), induced fractures can form when pieces of intact core are chipped off along the edges because of the plucking action of the clockwise-rotating drill bit.

Radiating fractures

Open fractures displaying a variety of orientations that radiate from, or seem to originate at, common points are observed in Hole C0019E cores and are inferred to be induced. This geometry is apparent in the split face and is consistent with formation in response to a load applied at an arbitrary angle and position where mismatched pieces of rock are in contact with intact core. Oftentimes the impacting fragment of rock is preserved, displaying a set of fractures that all radiate from the point of a triangular-shaped fragment (e.g., Fig. **F2G**). Similar radial arrays of fractures have been noted on previous IODP expeditions as being drilling induced. Arthur et al. (1980) and Dengo (1982) describe the fractures as originating near the core center with a radial symmetry in the downcore direction. Kulander et al. (1990) describe similar curviplanar fractures that originate outside of the core and diverge downcore. The point of origin for some radial fractures can therefore also be absent within the recovered core. However, an observation of the preserved impacting fragment is also evidence of mobile piece(s) of rock during the coring process. Radial fractures that originate off-core are an

indication of inception off-core and growth ahead of the advancing bit in rock that is subsequently drilled.

Core axis–parallel fractures

Several forms of induced deformation occur symmetrically about the long axis of the core. The most obvious of these is the presence of a zone of flowage (Dengo, 1982; Lundberg and Moore, 1986), rock fragments in a matrix of dominantly drilling mud between the core and the core liner. Additionally, two types of vertical induced fractures are recognized that vary in scale and orientation. The first are petal-centerline fractures, described in detail by Kulander et al. (1979, 1990) and Li and Schmitt (1998). Characteristic petal-centerline fractures dip between 30° and 75° in a downcore direction near the core edge and curve to dip vertically near the center of the core (Kulander et al., 1990). Petal-centerline fractures form in response to an induced principal tension that rotates downward in a vertical plane from an inclined orientation to horizontal (Kulander et al., 1979), and the strike of the fracture surface is aligned with the direction of the greatest horizontal stress (Li and Schmitt, 1998). We observe no clear petal-centerline fractures in the JFAST cores, similar to other studies in thrust faulting regimes (Li and Schmitt, 1998). However, in drill cores of well-indurated rock, petal-centerline fractures are commonly used to estimate in situ principal stress orientations (e.g., Li and Schmitt, 1998; Davatzes and Hickman, 2010).

The second type of core axis–parallel induced fractures is typically smaller in scale and interpreted as related to both the coring and handling processes. Induced core axis–parallel fractures, sometimes several centimeters in length and open several millimeters, are best observed in Section 20R-2 (Fig. **F2H**). This section, composed of dominantly stratified pelagic clay with subhorizontal bedding, displays subvertical fractures that appear to have originated near the center of the core and never reached the edge of the core. We interpret these induced fractures as forming under nonuniform deformation of layers under triaxial or uniaxial stress conditions, similar to "axial cracking" described in Dusseault and Van Domselaar (1984) and Kulander et al. (1990), where compression of the core vertically results in the formation of vertical to subvertical Mode I fractures that abut either a subhorizontal biscuit boundary or detachment surface within the core.

Small saw-mark–parallel fractures

Open fractures that are roughly 1 cm or less in length on the core face and aligned parallel to the ridges and grooves produced by the core-splitting saw are common. The fractures have nearly perfectly horizontal rakes along the cut face (Fig. **F2I**) and do not extend to the edge of the core. Most importantly, small saw-mark–parallel fractures cannot be observed in X-CT imagery collected before core splitting. Small horizontal fractures commonly terminate against other open fractures. Especially where they terminate against reactivated induced structures, the terminating fractures are likely younger in age and not related to tectonic deformation. The orientation of the fractures parallel to the saw blade and relative timing of formation of the fractures shows that they are handling-induced.

Drilling mud injection

Drilling mud may be difficult to distinguish from lithified (or partially lithified) clay and mudstone in cores. Drilling mud is typically lighter in color than the mudstone in Hole C0019E cores and is much softer. However, drilling mud can appear to be very similar to lighter rocks. In X-CT imagery, drilling mud is notably lighter than surrounding rocks because of the low density of the mud. Drilling mud correlates with induced deformation in a number of contexts. It can appear to have been injected through paths between drilling biscuits and is observed to penetrate along open fractures into the interior of the core. Small fragments of rock from cores can be entrained within the drilling mud matrix, giving the material the appearance of a breccia (Fig. **F2J**); however, such fragments cannot be considered tectonic in origin with any confidence without the presence of slickenlines. In these occurrences, a combination of biscuiting and drilling mud injection results in a drilling breccia.

Fractures crosscutting drilling mud

In rare instances, open fractures can be observed crosscutting drilling mud (Fig. **F2K**). The crosscutting and relative timing relationship is a clear indication that the fracture postdates the injection of drilling mud and therefore is induced by the drilling or coring processes.

Rubble

Commonly at the tops and bottoms of core sections is a total loss of coherence in the recovered rocks. The common location in the sections is not a coincidence because cores are often sectioned in places where this style of induced deformation occurs. Consequently, it is common for induced damage to be concentrated at the tops and bottoms of core sections and remain fairly evenly distributed through-

out the rest of the core. Subrounded fragments with a variety of lithologies and randomly oriented bedding appear as "rubble," a zone of fragments that are not in situ and likely each have entirely different origins (Fig. F2L). Rubble zones display no associated drilling mud at the top of core sections. Fragments in rubble zones rarely retain a cut face parallel to the orientation of core splitting.

Measurement of structure density

For the purposes of quantifying the density of structures in the examined cores, we categorized each structure based on a confidence index developed as part of this work. The first structural style (Category 1) is deformation that is unequivocally tectonic and in situ—the strongest possible confidence level regarding tectonic origin (see criteria outlined in "Distinguishing tectonic and induced deformation"). The second structural style (Category 2) is deformation that may be tectonic or induced in origin but lacks definitive evidence for either source. The third structural style (Category 3) is deformation that can clearly be demonstrated to have been induced by drilling, coring, and/or handling operations.

The density of core-scale structures was quantified using a linear scanline sampling method performed on core imagery and verified through direct observation of the archive halves. Structure density is defined here as a linear measurement of the number of structures per unit length (meters) (Rohrbaugh et al., 2002). High-resolution imagery of all cores was collected on board during Expedition 343 using a multisensor core logger (MSCL)-I digital imaging system with GEOSCAN IV (Geotek, Ltd.). The instrument uses a line-scan system for split-core imaging, reducing the optical distortion from the lens or variations of lighting and provides 16 bit RGB color TIFF-formatted images with a resolution of 100 pixels/cm. The linear scanline method allows for quick measurement of structure characteristics and is the main method used in borehole image logs and cores (Zeeb et al., 2013). The linear scanline method has been used in many previous studies of damage zone structures at the outcrop scale and has clearly documented elevated damage in the vicinity of many major faults (e.g., Caine and Forster, 1999; Wilson et al., 2003; Mitchell and Faulkner, 2009; Savage and Brodsky, 2011). In order to best avoid induced damage near the edge of the core, the linear scanline was drawn down the center of each core. The depth of every structure intersecting the scanline was recorded, and each structure was assigned a category according to the classification scheme described above.

In intensively deformed intervals of cores (i.e., breccia zones) where the spacing between structures was ~1 cm or less, depths of structures within the zone were approximated by estimating the average size of clasts within the zone. Because clasts within breccias are fragmented rock, the boundaries of clasts are fracture surfaces and the size of the clast is a measure of fracture spacing. We used an image analysis method implemented in Matlab following the methods of Bjørk et al. (2009) to measure clast properties. Because of the irregular sizes and shapes of clasts in breccia zones, the simple linear scanline sampling method could not completely represent the spacing of structures. We therefore calculated the average clast size in the breccia zone and set the structure density to the breccia interval thickness divided by the average clast diameter.

Results and discussion

The linear scanline intersected 2692 structures of all types over 16.11 m of examined core from Cores 10R–20R. Of these, 1102 were categorized as tectonic (Category 1), 1226 were clearly induced (Category 3), and 397 could not be shown to be either tectonic or induced (Category 2). Complete data for structure depths for all categories are included in STRUCTDEPTH in "Supplementary material." Each core contained structures that fell into all three categories (e.g., see Fig. F3, which shows the categorization method applied to structures in Section 14R-1).

Combining all three categories of structures in Hole C0019E cores, the results show the greatest structure density (measured as the number of structures per 20 cm depth interval) occurs adjacent to the Japan Trench plate boundary décollement (Fig. F4A). The largest structure density occurs near the décollement for all three of the structural categorizations (i.e., the same pattern is observed in calculations from exclusively Category 1 structures, summed Category 1 and 2, and summed Category 1, 2, and 3). In the hanging wall, local maxima for all three category combinations exceed 60 structures/m at ~819 mbsf. In the footwall, local maxima for all three category combinations surpass 80 structures/m at ~824 mbsf. These results show that high structure density correlates with the presence of the shallow Japan Trench décollement and an associated fault damage zone.

Throughout the interval of core spanned by our analysis, distinguishing trends in the spatial variability of structure density is dependent on the identification of induced structures. This is particularly the case in the hanging wall, where the structure density decreases with distance from the décollement for

Category 1 structures but not for the cumulative structure density of all three categories. For example, when induced deformation structures are included in the transect results shallower than 790 mbsf, the combined total of Categories 1–3 shows a slight increase in structure density. In contrast, the results for Category 1 structures without induced structures shows a significant decrease over the same interval. Including induced deformation structures therefore conceals the continued decay in tectonic structure density and could result in misinterpretation if high structure densities are used to define tectonic faults. In the footwall, inclusion of induced deformation makes the decay in structure density with distance from the décollement appear less steep than the decay in Category 1 structure density.

Secondary faults have associated minor damage zones that can result in locally high structure density around a major structure (Savage and Brodsky, 2011). Several major secondary faults defined by core observations (see the **"Expedition 343/343T summary"** chapter [Expedition 343/343T Scientists, 2013a]; Kirkpatrick et al., 2015), radiolarian biostratigraphic age ranges (see the **"Expedition 343/343T summary"** chapter [Expedition 343/343T Scientists, 2013a]), and/or chemostratigraphic constraints (Rabinowitz et al., 2015) are located in the transect interval (Fig. **F4A**). Of the major secondary faults, there are two types: (1) those identified within recovered core and (2) those inferred between cores in intervals that were not recovered. We observe slightly elevated tectonic structure density at ~817 and ~832 mbsf, corresponding to the locations of a secondary fault defined from core observations and chemostratigraphic constraints (Rabinowitz et al., 2015), respectively. At both depths, structure density decays both above and below the fault depth (see example from ~832 mbsf in Fig. **F4B**). Other secondary faults identified in recovered cores (~824.5 and ~825.2 mbsf) do not correlate with locally high tectonic structure density in our data. This is likely because the faults around 825 mbsf have small offsets, indicated by the lack of stratigraphic reversals or gaps associated with them (Rabinowitz et al., 2015). Secondary faults inferred between cores are not resolvable from our structure density data because of large gaps in core recovery and incomplete recovery within coring intervals.

Similar structure density data sets from previous ocean drilling expeditions have been used to investigate deformation in core (e.g., Brown and Behrmann, 1990; Maltman, et al., 1993; Saito et al., 2001). Our results show that the identification of induced structures and the confidence categorization method utilized in this study highlighted trends in tectonic deformation that would have been masked if induced deformation had been included. The induced structures described here are generic to drill core in sedimentary rocks, and the method we used could be applied in many tectonic settings, potentially enhancing the application of structure density characterization for detailed structural analysis.

Acknowledgments

Cores, images, and data used in this study were provided by the Integrated Ocean Drilling Program. Thanks to J. Casey Moore and J. Caine for providing constructive reviews of the manuscript. We thank the curatorial staff at the Kochi Core Center for their invaluable assistance and the visual core description team from Expedition 343 for extensive discussions that motivated our work. Funding for this study was provided by the National Science Foundation (award OCE 1260602).

References

Arthur, M.A., Carson, B., and von Huene, R., 1980. Initial tectonic deformation of hemipelagic sediment at the leading edge of the Japan convergent margin. *In* Langseth, M., Okada, H., et al., *Initial Reports of the Deep Sea Drilling Project,* 56, 57: Washington, DC (U.S. Government Printing Office), 569–613. **http://dx.doi.org/10.2973/dsdp.proc.5657.115.1980**

Bjørk, T.E., Mair, K., and Austrheim, H., 2009. Quantifying granular material and deformation: advantages of combining grain size, shape, and mineral phase recognition analysis. *Journal of Structural Geology,* 31(7):637–653. **http://dx.doi.org/10.1016/j.jsg.2009.03.020**

Brown, K.M., and Behrmann, J., 1990. Genesis and evolution of small-scale structures in the toe of the Barbados Ridge accretionary wedge. *In* Moore, J.C., Mascle, A., et al., *Proceedings of the Ocean Drilling Program, Scientific Results,* 110: College Station, TX (Ocean Drilling Program), 229–244. **http://dx.doi.org/10.2973/odp.proc.sr.110.141.1990**

Caine, J.S., and Forster, C.B., 1999. Fault zone architecture and fluid flow: insights from field data and numerical modeling. *In* Haneberg, W.C., Mozley, P.S., Moore, J.C., and Goodwin, L.B. (Eds.), *Faults and Subsurface Fluid Flow in the Shallow Crust*. Geophysical Monograph, 113:101–127. **http://dx.doi.org/10.1029/GM113p0101**

Caine, J.S., Evans, J.P., and Forster, C.B., 1996. Fault zone architecture and permeability structure. *Geology*, 24(11):1025–1028. **http://dx.doi.org/10.1130/0091-7613(1996)024<1025:FZAAPS>2.3.CO;2**

Chester, F.M., and Logan, J.M., 1986. Implications for mechanical properties of brittle faults from observa-

tions of the Punchbowl fault zone, California. *Pure and Applied Geophysics*, 124(1–2):79–106. **http://dx.doi.org/10.1007/BF00875720**

Davatzes, N.C., and Hickman, S.H., 2010. Stress, fracture, and fluid-flow analysis using acoustic and electrical image logs in hot fractured granites of the Coso Geothermal Field, California, U.S.A. *In* Pöppelreiter, M., Garcia-Carballido, C., and Kraaijveld, M. (Eds.), *Dipmeter and Borehole Image Log Technology*. AAPG Memoir, 92:259–293. **http://archives.datapages.com/data/specpubs/memoir92/CHAPTER15/CHAPTER15.HTM**

Dengo, C. 1982. A structural analysis of cores from the Leg 67 transect across the Middle America Trench—offshore Guatemala. *In* Aubuoin, J., von Huene, R., et al., (Eds.), *Initial Reports of the Deep Sea Drilling Project,* 67: Washington, DC (U.S. Government Printing Office), 651–666. **http://dx.doi.org/10.2973/dsdp.proc.67.133.1982**

Dusseault, M.B., and Van Domselaar, H.R., 1984. Unconsolidated sand sampling in Canadian and Venezuelan oil sands. *In* Meyer, R.F., Wynn, J.C., and Olson, J.C. (Eds.), *The Future of Heavy Crude and Tar Sands: The Second International Conference:* New York (McGraw-Hill), 336–348.

Expedition 343/343T Scientists, 2013a. Expedition 343/343T summary. *In* Chester, F.M., Mori, J., Eguchi, N., Toczko, S., and the Expedition 343/343T Scientists, *Proceedings of the Integrated Ocean Drilling Program,* 343/343T: Tokyo (Integrated Ocean Drilling Program Management International, Inc.). **http://dx.doi.org/10.2204/iodp.proc.343343T.101.2013**

Expedition 343/343T Scientists, 2013b. Methods. *In* Chester, F.M., Mori, J., Eguchi, N., Toczko, S., and the Expedition 343/343T Scientists, *Proceedings of the Integrated Ocean Drilling Program,* 343/343T: Tokyo (Integrated Ocean Drilling Program Management International, Inc.). **http://dx.doi.org/10.2204/iodp.proc.343343T.102.2013**

Fossen, H., Schultz, R.A., Shipton, Z.K., and Mair, K., 2007. Deformation bands in sandstone: a review. *Journal of the Geological Society (London, U. K.)*, 164(4):755–769. **http://dx.doi.org/10.1144/0016-76492006-036**

Fujii, Y., Satake, K., Sakai, S., Shinohara, M., and Kanazawa, T., 2011. Tsunami source of the 2011 off the Pacific coast of Tohoku earthquake. *Earth, Planets Space,* 63(7):815–820. **http://dx.doi.org/10.5047/eps.2011.06.010**

Fujiwara, T., Kodaira, S., No, T., Kaiho, Y., Takahashi, N., and Kaneda, Y., 2011. The 2011 Tohoku-Oki earthquake: displacement reaching the trench axis. *Science,* 334(6060):1240. **http://dx.doi.org/10.1126/science.1211554**

Hiraishi, H., 1984. Evaluation of shear and flexural deformations of flexural type shear walls. *Bulletin of the New Zealand Society for Earthquake Engineering,* 17(2):135–144.

Ide, S., Baltay, A., and Beroza, G.C., 2011. Shallow dynamic overshoot and energetic deep rupture in the 2011 M_w 9.0 Tohoku-Oki earthquake. *Science,* 332(6036):1426–1429. **http://dx.doi.org/10.1126/science.1207020**

Kidd, R.B., 1978. Core-discing and other drilling effects in DSDP Leg 42A Mediterranean sediment cores. *In* Hsu, K., Montadert, L. et al. (Eds.), *Initial Reports of the Deep Sea Drilling Project,* 42 Part 1: Washington, DC (U.S. Government Printing Office), 1143–1149. **http://dx.doi.org/10.2973/dsdp.proc.42-1.app1.1978**

Kirkpatrick, J.D., Rowe, C.D., Ujiie, K., Moore, J.C., Regalla, C., Remitti, F., Toy, V., Wolfson-Schwehr, M., Kameda, J., Bose, S., and Chester, F.M., 2015. Structure and lithology of the Japan Trench subduction plate boundary fault. *Tectonics,* 34(1):53–69. **http://dx.doi.org/10.1002/2014TC003695**

Kulander, B.R., Barton, C.C., and Dean, S.L., 1979. *The Application of Fractography to Core and Outcrop Fracture Investigations* (U.S. DOE Report METC/SP-79/3): Morgantown, WV (US Government Printing Office). **http://corescholar.libraries.wright.edu/ees/107**

Kulander, B.R., Dean, S.L., and Ward, B.J., Jr., 1990. *AAPG Methods in Exploration* (Volume 8): *Fractured Core Analysis: Interpretation, Logging, and Use of Natural and Induced Fractures in Core:* Tulsa, OK (AAPG).

Lay, T., Ammon, C.J., Kanamori, H., Xue, L., and Kim, M.J., 2011. Possible large near-trench slip during the 2011 M_w 9.0 off the Pacific coast of Tohoku earthquake. *Earth, Planets and Space*, 63(7):687–692. **http://dx.doi.org/10.5047/eps.2011.05.033**

Leggett, J.K., 1982. Drilling-induced structures in Leg 66 cores. *In* Mariana, L., et al. (Eds.) *Initial Reports of the Deep Sea Drilling Project,* 66: Washington, DC (U.S. Government Printing Office), 531–538. **http://dx.doi.org/10.2973/dsdp.proc.66.118.1982**

Li, Y., and Schmitt, D.R., 1998. Drilling-induced core fractures and in situ stress. *Journal of Geophysical Research: Solid Earth,* 103(B3):5225–5239. **http://dx.doi.org/10.1029/97JB02333**

Lundberg, N., and Moore, J.C., 1986. Macroscopic structural features in Deep Sea Drilling Project cores from forearc regions. *In* Moore, J.C. (Ed.), *Structural Fabric in Deep Sea Drilling Project Cores From Forearcs*. Memoirs—Geological Society of America, 166:13–44. **http://dx.doi.org/10.1130/mem166-p13**

Maltman, A.J., Byrne, T., Karig, D.E., and Lallemant, S., 1993. Deformation at the toe of an active accretionary prism: synopsis of results from ODP Leg 131, Nankai, SW Japan. *Journal of Structural Geology,* 15(8):949–964. **http://dx.doi.org/10.1016/0191-8141(93)90169-B**

Mitchell, T.M., and Faulkner, D.R., 2009. The nature and origin of off-fault damage surrounding strike-slip fault zones with a wide range of displacements: a field study from the Atacama fault system, northern Chile. *Journal of Structural Geology*, 31(8):802–816. **http://dx.doi.org/10.1016/j.jsg.2009.05.002**

Mori, J., Chester, F.M., Eguchi, N., and Toczko, S., 2012. Japan Trench Fast Earthquake Drilling Project (JFAST). *Integrated Ocean Drilling Program Scientific Prospectus,* 343. **http://dx.doi.org/10.2204/iodp.sp.343.2012**

Nakamura, Y., Kodaira, S., Cook, B.J., Jeppson, T., Kasaya, T., Yamamoto, Y., Hashimoto, Y., Yamaguchi, M., Obana, K., and Fujie, G., 2014. Seismic imaging and velocity structure around the JFAST drill site in the

Japan Trench: low *Vp*, high *Vp*/*Vs* in the transparent frontal prism. *Earth, Planets and Space,* 66:121. **http://dx.doi.org/10.1186/1880-5981-66-121**

Nakamura, Y., Kodaira, S., Miura, S., Regalla, C., and Takahashi, N., 2013. High-resolution seismic imaging in the Japan Trench axis area off Miyagi, northeastern Japan. *Geophysical Research Letters,* 40(9):1713–1718. **http://dx.doi.org/10.1002/grl.50364**

Pendexter, C., and Rohn, R.E., 1954. Fractures induced during drilling. *Journal of Petroleum Technology*, 6(3):15.

Pollitz, F.F., Bürgmann, R., and Banerjee, P., 2011. Geodetic slip model of the 2011 M9.0 Tohoku earthquake. *Geophysical Research Letters*, 38(7):L00G08. **http://dx.doi.org/10.1029/2011gl048632**

Rabinowitz, H.S., Savage, H.M., Plank, T., Polissar, P.J., Kirkpatrick, J.D., and Rowe, C.D., 2015. Multiple major faults at the Japan Trench: chemostratigraphy of the plate boundary at IODP Exp. 343: JFAST. *Earth and Planetary Science Letters,* 423:57–66. **http://dx.doi.org/10.1016/j.epsl.2015.04.010**

Rohrbaugh, M.B., Jr., Dunne, W.M., and Mauldon, M., 2002. Estimating fracture trace intensity, density, and mean length using circular scan lines and windows. *AAPG Bulletin,* 86(12):2089–2014. **http://dx.doi.org/10.1306/61eede0e-173e-11d7-8645000102c1865d**

Saito, S., Goldberg, D., and Leg 196 Shipboard Scientific Party, 2001. *ODP Leg 196: Deformation and Fluid Flow Processes in the Nankai Trough Accretionary Prism, Downhole Logging Summary*. **http://www.ldeo.columbia.edu/BRG/ODP/ODP/LEG_SUMM/196/leg196.html**

Savage, H.M., and Brodsky, E.E., 2011. Collateral damage: evolution with displacement of fracture distribution and secondary fault strands in fault damage zones. *Journal of Geophysical Research: Solid Earth,* 116(B3):B03405. **http://dx.doi.org/10.1029/2010JB007665**

Ujiie, K., and Kimura, G., 2014. Earthquake faulting in subduction zones: insights from fault rocks in accretionary prisms. *Progress in Earth and Planetary Science,* 1:7–37. **http://dx.doi.org/10.1186/2197-4284-1-7**

Wilson, J.E., Chester, J.S., and Chester, F.M., 2003. Microfracture analysis of fault growth and wear processes, Punchbowl Fault, San Andreas system, California. *Journal of Structural Geology*, 25(11):1855–1873. **http://dx.doi.org/10.1016/s0191-8141(03)00036-1**

Yue, H., and Lay, T., 2011. Inversion of high-rate (1 sps) GPS data for rupture process of the 11 March 2011 Tohoku earthquake (M_w 9.1). *Geophysical Research Letters,* 38(7):L00G09. **http://dx.doi.org/10.1029/2011gl048700**

Zeeb, C., Gomez-Rivas, E., Bons, P.D., and Blum, P., 2013. Evaluation of sampling methods for fracture network characterization using outcrops. *AAPG Bulletin,* 97(9):1545–1566. **http://dx.doi.org/10.1306/02131312042**

Initial receipt: 22 January 2015
Acceptance: 1 December 2015
Publication: 4 March 2016
MS 343343T-204

Figure F1. A. Location map showing Tohoku area of the Japan Trench and Tohoku-oki earthquake epicenter. **B.** Location of Site C0019 and orientation of in-line seismic section Line HD34B (Nakamura et al., 2013) (500 m north of Site C0019) (modified after Fig. F1 in the "Expedition 343/343T summary" chapter [Expedition 343/343T Scientists, 2013a]). **C.** Cross section (A to A′) through the toe of the Japan Trench prism with location of Site C0019 and plate boundary décollement showing overall margin architecture (V.E. = vertical exaggeration) (modified after Kirkpatrick et al., 2015).

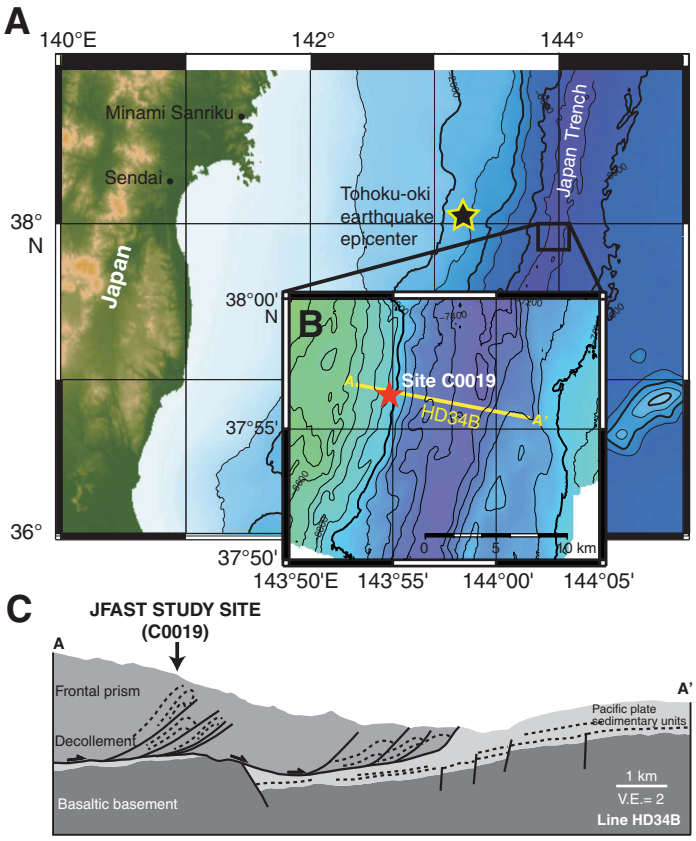

Figure F2. Examples of induced structure types observed in Hole C0019E cores. White arrows = feature exemplified in image. **A.** Induced biscuit/disc fracture with characteristic arched bottom. All scales are in cm. **B.** Induced brecciation below white line, with characteristic angular, randomly oriented clasts exhibiting no slickenlines. **C.** Two low-angle triangular fracture sets in which the internal piece of rock bound by the fractures no longer remains. **D.** High-angle triangular fracture set in which internal piece of rock remains. **E.** Triangular fracture set in which the fracture with an apparent dip to the right of the photo has opened along a preexisting tectonic structure (denoted with dashed white line). **F.** Two approximately right angle fracture sets near bottom edge of an induced biscuit/disc. The fracture with an apparent steep dip to the right of the photo has opened along a preexisting tectonic structure (dashed white line). **G.** Radial fracture set (dashed white lines) propagating from an impact point likely at the location of the white arrow. **H.** Subvertical fractures in the pelagic clay at the base of Section 20R-2. **I.** Small saw-mark–parallel fractures that open in the same orientation as the horizontal saw-mark striations in the upper right portion of the photo. **J.** Induced fractures resulting from drilling mud injection. Drilling mud has a characteristic bright color that matches the fill in the fractures identified with white arrows. **K.** Open fracture crosscutting a zone of drilling mud injection. **L.** Zone of rubble, characteristically at the top of a core section with randomly oriented, mismatched fragments with no slickenlines.

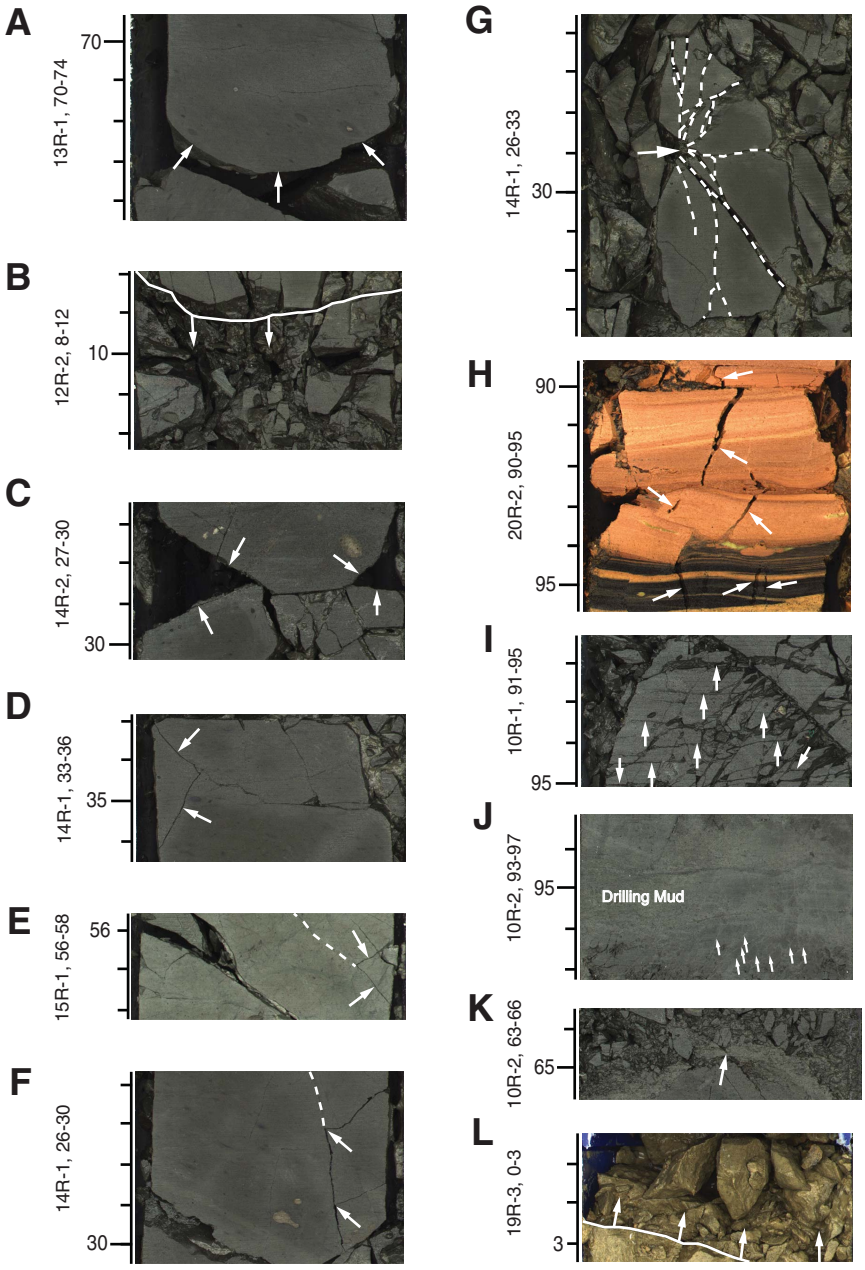

Figure F3. A. High-resolution MCSL-I photograph of Section 14R-1 archive half, cropped at wavy black line to exclude sampled portion of core between 53 and 85 cm (where imagery is unavailable). **B.** Same core section digitized with structure traces and types based on confidence categorization method (blue lines = Category 1 structures, red lines = Category 2 structures, white lines = Category 3 structures).

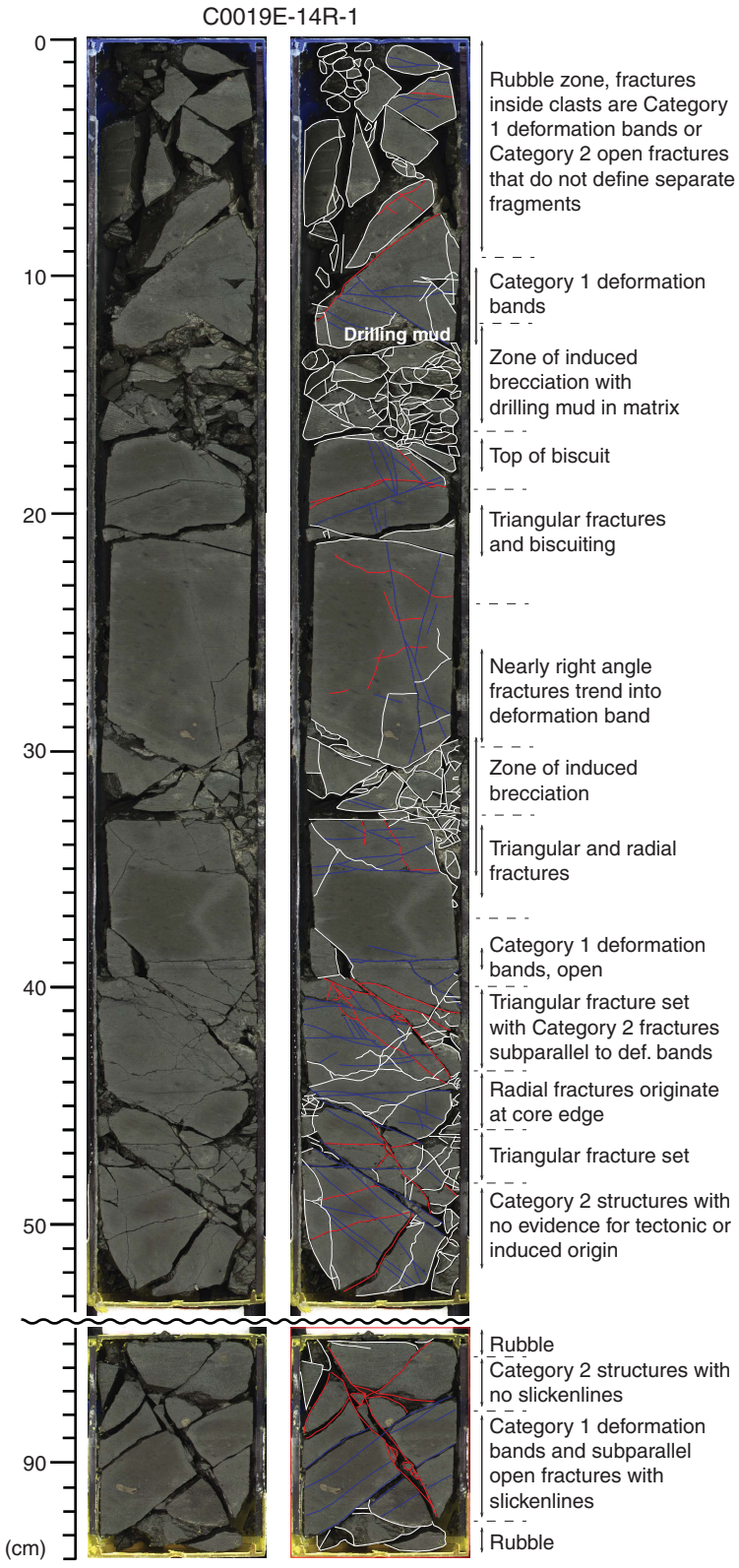

Figure F4. A. Number of structures (per 20 cm bin). Arrows = depths of known secondary faults, most of which are not resolvable from tectonic structure density data. **B.** Detail of the location of the secondary fault identified from chemostratigraphy showing the corresponding structure density data. A small increase in tectonic structure density is centered on the secondary fault.